



Shock waves in relativistic anisotropic hydrodynamics

Aleksandr Kovalenko^a, Andrei Leonidov^b

P.N. Lebedev Physical Institute, Moscow, Russia

Received: 7 October 2021 / Accepted: 19 April 2022 / Published online: 29 April 2022
© The Author(s) 2022

Abstract Shock wave solutions in anisotropic relativistic hydrodynamics are analysed. A new phenomenon of anisotropy-related angular deflection of the incident flow by the shock wave front is described. Patterns of velocity and momentum transformation by the shock wave front are described.

1 Introduction

The physics of ultrarelativistic heavy ion collisions is to a large extent determined by that of the Little Bang – evolution of hot and dense predominantly gluon matter created at the initial stage of these collisions, see [1] for a recent review. One of the characteristic features of this early evolution is a large pressure anisotropy due to formation of glasma flux tubes [2]. A standard way of describing expansion, cooling and subsequent transformation into final hadrons is to use the framework of relativistic dissipative hydrodynamics, see e.g. [3–5]. The large difference between longitudinal and transverse pressure leads to a necessity of going beyond standard viscous hydrodynamics by summing over velocity gradients to all orders. A candidate theory of this sort is relativistic anisotropic hydrodynamics, see e.g. [6,7] and the review papers [8–10] covering its both theoretical and phenomenological aspects. A non-additive generalisation of relativistic anisotropic hydrodynamics was recently suggested in [11]. To analyse possible physical consequences of the pressure anisotropy it is of interest to study the anisotropic versions of specific phenomena such as sound propagation and shock waves.

Sound propagation and Mach cone formation in anisotropic relativistic hydrodynamics was considered in [12]. The present paper is devoted to the analysis of shock wave solutions. The shock wave solutions in ideal relativistic hydro-

dynamics are known for a long time, see e.g. [13–15]. As to the viscous relativistic hydrodynamics, the shock wave solutions in its Israel-Stewart version were shown to exist only for small Mach numbers, i.e. for weak shock waves [16,17]. It is therefore interesting that shock wave solutions for anisotropic relativistic hydrodynamics (i.e. for a theory including gradients of velocity to all orders) considered in the present paper are constructed as direct generalization of the corresponding solutions in the ideal relativistic hydrodynamics and are valid for arbitrarily strong shock waves.

In applications to heavy ion physics the effects of shock waves were mostly discussed for low energy collisions [18–20]. An important exception is the study of [21,22] of transverse shock waves generated in the primordial turbulent gluon/minijet medium in high energy heavy ion collisions. With modern glasma type understanding of the essentially anisotropic nature of this medium it is of interest to rethink the results of [21,22] in terms of transverse shocks generated in anisotropic relativistic hydrodynamics. The present paper is a first step in this direction.

2 Shock waves in anisotropic relativistic hydrodynamics

2.1 Shock wave discontinuity in isotropic relativistic hydrodynamics

In this section we set the framework of subsequent analysis by reminding of the necessary information on shock wave discontinuity in isotropic relativistic hydrodynamics [13–15]. We focus on the shock wave solution in the ideal fluid characterised by the energy-momentum tensor

$$T_{\mu\nu} = (\varepsilon + P)U^\mu U^\nu - Pg^{\mu\nu} \quad (1)$$

where ε is energy density, P is the pressure and U^μ is the four-vector of the flow velocity satisfying $U_\mu U^\mu = 1$. In this case, the shock wave is described by a discontinuous solution of the equations of motion such that components of energy-

^a e-mail: kovalenkoam@lebedev.ru

^b e-mail: leonidovav@lebedev.ru (corresponding author)

momentum tensor normal to the discontinuity hypersurface are discontinuous across it while tangential ones remain continuous.

The energy–momentum conservation then leads to the following matching condition linking downstream and upstream projections on the direction perpendicular to the discontinuity surface:

$$T_{\mu\nu}N^\mu = T'_{\mu\nu}N^\mu, \tag{2}$$

where N^μ - unit vector normal to the discontinuity surface and $T_{\mu\nu}$ and $T'_{\mu\nu}$ correspond to upstream and downstream energy–momentum tensors correspondingly.

A quantitative description of a shock wave is that of a transformation of pressure, entropy S and normal component of velocity v across the shock wave surface:

$$(P, S, v) \Rightarrow (P', S', v'). \tag{3}$$

In this paper we will consider only the case of a compression shock wave for which $P' > P$, $S' > S$ and $v' < v$ (see a detailed derivation of the expression for the velocity drop below). The ratio $\sigma = P'/P$ will be considered as a parameter characterising the shock wave solution.

Using the explicit expression the energy–momentum tensor (1) we get

$$(\varepsilon + P)U_\mu N^\mu U_\nu - PN_\nu = (\varepsilon' + P')U'_\mu N^\mu U'_\nu - P'N_\nu. \tag{4}$$

Taking the product of Eq. (4) with U^ν and U'^ν one can obtain the following system:

$$(\varepsilon + P')x = (\varepsilon' + P')Ax', \tag{5}$$

$$(\varepsilon' + P)x' = (\varepsilon + P)Ax, \tag{6}$$

where we have defined $x = U_\mu N^\mu$, $x' = U'_\mu N^\mu$ and $A = U'_\nu U^\nu$. We get

$$(\varepsilon + P')(\varepsilon + P)x^2 = (\varepsilon' + P)(\varepsilon' + P')x'^2. \tag{7}$$

The vector N^μ must be space-like, $N^\mu N_\mu < 0$, for discontinuity surface to propagate inside the light cone and thus be subluminal [14]. After multiplying equation (4) by N_μ one finds

$$N_\nu N^\nu = \frac{1}{P - P'} [(\varepsilon + P)x^2 - (\varepsilon' + P')x'^2], \tag{8}$$

and, using (7) one gets

$$N_\mu N^\mu = \frac{\varepsilon' + P'}{\varepsilon + P} \left[1 - \frac{\varepsilon - \varepsilon'}{P - P'} \right] = \frac{\varepsilon + P}{\varepsilon' + P} \left[1 - \frac{\varepsilon - \varepsilon'}{P - P'} \right]. \tag{9}$$

The sublimality condition $N_\mu N^\mu < 0$ is thus insured by the following inequality

$$\frac{\varepsilon - \varepsilon'}{P - P'} > 1. \tag{10}$$

In ultra-relativistic case, then $\varepsilon = 3P$, the inequality (10) is trivially satisfied.

For the discussion below it is useful to remind an expression for the upstream and downstream velocities [15] in the ultrarelativistic case. Choosing $N^\mu = (0, 1, 0, 0)$ and 4-velocity vector of the form $U^\mu = (U^0, U_x, 0, 0)$ we get:

$$4PU_x U_0 = 4P'U'_x U'_0, \tag{11}$$

$$-4PU_x^2 - P = -4P'U_x'^2 - P'. \tag{12}$$

so that in terms in terms of the velocity components $v_i = U_i/U_0$

$$v_x = \sqrt{\frac{3\sigma + 1}{3(\sigma + 3)}}, \quad v'_x = \sqrt{\frac{\sigma + 3}{3(3\sigma + 1)}}. \tag{13}$$

A compact characterisation of the velocity transformation (13) across the shock wave front is given by relative difference between upstream and downstream velocities

$$\delta_{\text{iso}} = \frac{v'_x - v_x}{v_x} = -\frac{2}{3\sigma + 1}(\sigma - 1) \tag{14}$$

For the considered case of a compression shock wave $P' > P$ one has $\sigma > 1$ and, therefore, it follows from (14) that $\delta_{\text{iso}} < 0$ so that the flow velocity indeed drops across the compression shock wave front. Let us also note that

$$\rho_{\text{iso}} = v_x v'_x = \frac{1}{3} = c_s^2 \tag{15}$$

where c_s is a speed of sound.

One of the main topics of the analysis below is the one of the velocity transformation $\mathbf{v} \rightarrow \mathbf{v}'$ in anisotropic relativistic hydrodynamics generalising the formulae (14) and (15) for the isotropic case.

2.2 Anisotropic relativistic hydrodynamics

Our treatment of anisotropic relativistic hydrodynamics will follow the kinetic theory – founded approach of [6,23,24] based on working with a specific ansatz for a distribution function

$$f(x, p) = f_{\text{iso}} \left(\frac{\sqrt{p^\mu \mathcal{E}_{\mu\nu}(x) p^\nu}}{\Lambda(x)} \right), \tag{16}$$

where $\Lambda(x)$ is a coordinate-dependent temperature-like momentum scale and $\mathcal{E}_{\mu\nu}(x)$ quantifies coordinate-dependent

momentum anisotropy. In what follows we consider one-dimensional anisotropy so that $(p^\mu \Xi_{\mu\nu} p^\nu = \mathbf{p}^2 + \xi(x) p_\parallel^2)$ in the local rest frame (LRF). To obtain a transparent parametrisation of the energy–momentum tensor in anisotropic hydrodynamics it is convenient to rewrite the four-vector $U^\mu(x)$ in terms of the longitudinal rapidity $\vartheta(x)$, the timelike velocity u_0 and transverse velocities u_x, u_y

$$U^\mu = (u_0 \cosh \vartheta, u_x, u_y, u_0 \sinh \vartheta) \tag{17}$$

where $u_0^2 = 1 + u_x^2 + u_y^2$ and define a space-like unit vector

$$Z^\mu = (\sinh \vartheta, 0, 0, \cosh \vartheta) \tag{18}$$

such that $Z^\mu Z_\mu = -1$ which is orthogonal to U^μ , $Z_\mu U^\mu = 0$.

Using a standard definition for energy-momentum tensor as the second moment of the distribution function

$$T^{\mu\nu} = \int \frac{d^3 p}{(2\pi)^2 p_0} p^\mu p^\nu f_{iso} \left(\frac{\sqrt{p^\mu \Xi_{\mu\nu}(x) p^\nu}}{\Lambda(x)} \right) \tag{19}$$

one can derive the following equation for the energy-momentum tensor $T^{\mu\nu}$:

$$T^{\mu\nu} = (\varepsilon + P_\perp) U^\mu U^\nu - P_\perp g^{\mu\nu} + (P_\parallel - P_\perp) Z^\mu Z^\nu, \tag{20}$$

P_\parallel and P_\perp is longitudinal (towards anisotropy direction) and transverse pressure respectively. In the LRF the expression (20) takes the form

$$T^{\mu\nu} = \text{diag}(\varepsilon, P_\perp, P_\perp, P_\parallel) \tag{21}$$

Let us note that in the ultra-relativistic case the condition of the tracelessness of the energy-momentum tensor leads to the relation $\varepsilon = 2P_\perp + P_\parallel$.

The dependence on the anisotropy parameter ξ can be factorised so that

$$\varepsilon = \int \frac{d^3 p}{(2\pi)^2} p^0 f_{iso} \left(\frac{\sqrt{\mathbf{p}^2 + \xi(x) p_\parallel^2}}{\Lambda(x)} \right) = R(\xi) \varepsilon_{iso}(\Lambda), \tag{22}$$

$$P_\perp = \int \frac{d^3 p}{(2\pi)^2} \frac{p_\perp^2}{2p_0} f_{iso} \left(\frac{\sqrt{\mathbf{p}^2 + \xi(x) p_\parallel^2}}{\Lambda(x)} \right) = R_\perp(\xi) P_{iso}(\Lambda), \tag{23}$$

$$P_\parallel = \int \frac{d^3 p}{(2\pi)^2} \frac{p_\parallel^2}{p_0} f_{iso} \left(\frac{\sqrt{\mathbf{p}^2 + \xi(x) p_\parallel^2}}{\Lambda(x)} \right) = R_\parallel(\xi) P_{iso}(\Lambda), \tag{24}$$

where the anisotropy-dependent factors $R_\perp(\xi)$ and $R_\parallel(\xi)$ read [23, 24]

$$R_\perp(\xi) = \frac{3}{2\xi} \left(\frac{1 + (\xi^2 - 1)R(\xi)}{1 + \xi} \right),$$

$$R_\parallel(\xi) = \frac{3}{\xi} \left(\frac{(\xi + 1)R(\xi) - 1}{1 + \xi} \right), \tag{25}$$

where, in turn,

$$R(\xi) = \frac{1}{2} \left(\frac{1}{1 + \xi} + \frac{\arctan \sqrt{\xi}}{\sqrt{\xi}} \right). \tag{26}$$

Let us note that the anisotropy factors (25, 26) are related by the following useful formula:

$$2R_\perp(\xi) + R_\parallel(\xi) = 3R(\xi) \tag{27}$$

In the preceding paper [12] we have derived the following equation describing propagation of sound in relativistic anisotropic hydrodynamics with longitudinal anisotropy:

$$\partial_t^2 n^{(1)} = \left(c_{s\perp}^2 \partial_\perp^2 + c_{s\parallel}^2 \partial_z^2 \right) n^{(1)} \tag{28}$$

where $n^{(1)}$ is a (small) density fluctuation and $c_{s\perp}$ and $c_{s\parallel}$ stand for anisotropy-dependent transverse and longitudinal speed of sound respectively. The explicit expressions for $c_{s\perp}^2$ and $c_{s\parallel}^2$ read [12]:

$$c_{s\perp}^2 = \frac{R_\perp}{2R_\perp + R_\parallel}, \quad c_{s\parallel}^2 = \frac{R_\parallel}{2R_\perp + R_\parallel}. \tag{29}$$

Using Eq. (27) the expressions (29) can be rewritten in the following simple form:

$$c_{s\perp}^2 = \frac{R_\perp}{3R}, \quad c_{s\parallel}^2 = \frac{R_\parallel}{3R} \tag{30}$$

2.3 Transverse and longitudinal shock waves

2.3.1 Transverse normal shock wave

Let us first consider a description of a transverse shock wave. Due to the symmetry in Oxy -plane, it sufficient to consider its propagation along the x axis and, correspondingly, choose the following basis:

$$U_\mu = (u_0, u_x, 0, 0), \quad Z_\mu = (0, 0, 0, 1), \tag{31}$$

$$U'_\mu = (u'_0, u'_x, 0, 0), \quad Z'_\mu = Z_\mu = (0, 0, 0, 1). \tag{32}$$

Similarly to the example from relativistic hydrodynamics, consider the case when the normal vector is directed along the Ox -axis $N^\mu = (0, 1, 0, 0)$ (solution for the case of an arbitrary N^μ see Appendix B). In the ultrarelativistic case The matching conditions (2) then lead to the following system of equations:

$$(3P_\perp + P_\parallel)u_0 u_x - (3P'_\perp + P'_\parallel)u'_0 u'_x = 0, \tag{33}$$

$$(3P_\perp + P_\parallel)u_x^2 + P_\perp - (3P'_\perp + P'_\parallel)(u'_x)^2 - P'_\perp = 0. \tag{34}$$

From the Eqs. (33–34) we find expressions for the velocities u_x, u'_x :

$$u_x = \frac{v_x}{u_0} = \sqrt{\frac{(P_{\perp} - P'_{\perp})(P'_{\parallel} + P_{\perp} + 2P'_{\perp})}{(2P_{\perp} - P_{\parallel} - 2P'_{\perp} + P'_{\parallel})(P'_{\parallel} + 2P_{\perp} + P'_{\perp})}}, \tag{35}$$

$$u'_x = \frac{v'_x}{u'_0} = \sqrt{\frac{(P_{\perp} - P'_{\perp})(P'_{\parallel} + 2P_{\perp} + P'_{\perp})}{(2P_{\perp} - P_{\parallel} - 2P'_{\perp} + P'_{\parallel})(P'_{\parallel} + P_{\perp} + 2P'_{\perp})}}, \tag{36}$$

It is assumed that the anisotropy parameter does not change near the shock wave, since anisotropy is related to the properties of the medium, thus $\xi' = \xi$. Using the formulae (13)–(26) for the transverse and longitudinal pressure and anisotropy factors one gets the following expressions for the upstream and downstream velocities v_x and v'_x :

$$\begin{aligned} v_x(\sigma, \xi) &= \sqrt{\frac{R_{\perp}(3\sigma R + R_{\perp})}{3R(R_{\perp}\sigma + 3R)}}, \\ v'_x(\sigma, \xi) &= \sqrt{\frac{R_{\perp}(R_{\perp}\sigma + 3R)}{3R(3\sigma R + R_{\perp})}}, \end{aligned} \tag{37}$$

where, as before, $\sigma = P'_{iso}/P_{iso}$.

Using the expressions (37) we can calculate the relative difference $\delta_{\perp}(\xi|\sigma)$ and the product $\rho_{\perp}(\xi)$ of the upstream and downstream velocities

$$\delta_{\perp}(\xi|\sigma) = \frac{v'_x - v_x}{v_x} = -(\sigma - 1) \frac{3R - R_{\perp}}{3\sigma R + R_{\perp}} \tag{38}$$

$$\rho_{\perp}(\xi) = v_x v'_x = \frac{R_{\perp}}{3R}. \tag{39}$$

Let us note that the dependence on σ of the velocities (37) cancels in their product $\rho_{\perp}(\xi)$ in (39).

Recalling the fact that the product of upstream and downstream velocities in the isotropic case is equal to the speed of sound squared, see Eq. (15), one can identify such a product for the transverse shock wave with a transverse speed of sound squared

$$\rho_{\perp}(\xi) = c_{s\perp}^2 \tag{40}$$

Comparing Eq. (39) and the first equation in (30) we see that this definition leads to an expression identical to that following from the equation for sound propagation in relativistic anisotropic hydrodynamics derived in [12].

In the isotropic limit $\xi \rightarrow 0$

$$\delta_{\perp}(\xi|\sigma)|_{\xi \rightarrow 0} \rightarrow \delta_{iso}, \quad \rho_{\perp}(\xi)|_{\xi \rightarrow 0} \rightarrow \rho_{iso}, \tag{41}$$

where δ_{iso} and ρ_{iso} were defined in Eqs. (14) and (15).

In the opposite limit of $\xi \rightarrow \infty$

$$\delta_{\perp}(\xi|\sigma)|_{\xi \rightarrow \infty} \rightarrow -(\sigma - 1) \frac{1}{2\sigma + 1}, \quad \rho_{\perp}(\xi)|_{\xi \rightarrow \infty} \rightarrow \frac{1}{2}, \tag{42}$$

The functions $\delta_{\perp}(\xi|\sigma)$ and $\rho_{\perp}(\xi)$ are plotted in Figs. 1, and 2.

2.3.2 Longitudinal normal shock wave

Similar calculations can be carried out for the longitudinal shock wave propagating along the anisotropy axis. In this case we choose

$$U_{\mu} = (\cosh \vartheta, 0, 0, \sinh \vartheta), \quad Z_{\mu} = (\sinh \vartheta, 0, 0, \cosh \vartheta). \tag{43}$$

Proceeding analogously to the previously considered case for the transverse shock wave we get

$$\begin{aligned} v_z(\sigma, \xi) &= \sqrt{\frac{R_{\parallel}(3\sigma R + R_{\parallel})}{3R(R_{\parallel}\sigma + 3R)}}, \\ v'_z(\sigma, \xi) &= \sqrt{\frac{R_{\parallel}(R_{\parallel}\sigma + 3R)}{3R(3\sigma R + R_{\parallel})}}. \end{aligned} \tag{44}$$

The corresponding expressions for $\delta_{\parallel}(\xi|\sigma)$ and $\rho_{\parallel}(\xi)$ read

$$\delta_{\parallel}(\xi) = \frac{v'_z - v_z}{v_z} = -(\sigma - 1) \frac{3R - R_{\parallel}}{3\sigma R + R_{\parallel}} \tag{45}$$

$$\rho_{\parallel}(\xi) = v_z v'_z = \frac{R_{\parallel}}{3R} \tag{46}$$

Defining analogously to (40)

$$\rho_{\parallel}(\xi) = c_{s\parallel}^2 \tag{47}$$

and comparing Eq. (46) with the second equation in (30) we see that like in the transverse case this definition leads to an expression identical to that following from the equation for sound propagation in relativistic anisotropic hydrodynamics derived in [12].

In the isotropic limit $\xi \rightarrow 0$

$$\delta_{\parallel}(\xi|\sigma)|_{\xi \rightarrow 0} \rightarrow \delta_{iso}, \quad \rho_{\parallel}(\xi)|_{\xi \rightarrow 0} \rightarrow \rho_{iso}. \tag{48}$$

In the opposite limit of $\xi \rightarrow \infty$

$$\delta_{\parallel}(\xi|\sigma)|_{\xi \rightarrow \infty} \rightarrow -(\sigma - 1) \frac{1}{\sigma}, \quad \rho_{\parallel}(\xi)|_{\xi \rightarrow \infty} \rightarrow 0. \tag{49}$$

The functions $\delta_{\parallel}(\xi|\sigma)$ and $\rho_{\parallel}(\xi)$ are plotted, together with their counterparts $\delta_{\perp}(\xi|\sigma)$ and $\rho_{\perp}(\xi)$, in Figs. 1, and 2.

2.3.3 Comparison between normal transverse and longitudinal shock waves

From Figs. 1, and 2 we see that the anisotropy dependence of the relative rapidity drop $\delta_{\perp}(\xi|\sigma)$ and velocities product $\rho_{\perp}(\xi)$ and that of their longitudinal counterparts $\delta_{\parallel}(\xi|\sigma)$ and $\rho_{\parallel}(\xi)$ are of different character. We see in particular that

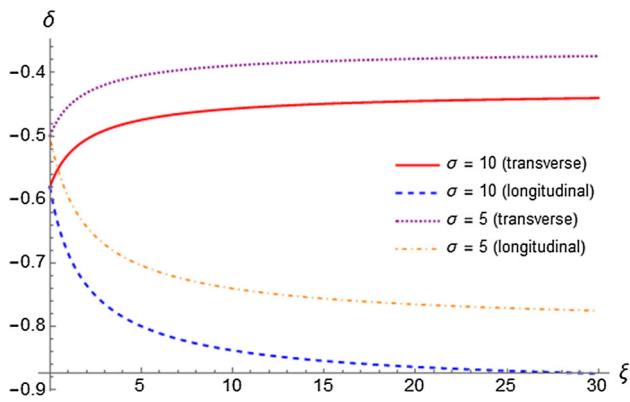


Fig. 1 Plot of the relative velocity differences $\delta_{\perp}(\xi|\sigma)$ (38) for $\sigma = 5$ (dotted line) and $\sigma = 10$ (solid line) and $\delta_{\parallel}(\xi|\sigma)$ (45) for $\sigma = 5$ (dash-dotted line) and $\sigma = 10$ (dashed line) as functions of the anisotropy parameter ξ . A decrease (increase) in $\delta_{\perp,\parallel}(\xi|\sigma)$ indicates weakening (strengthening) of the shock wave

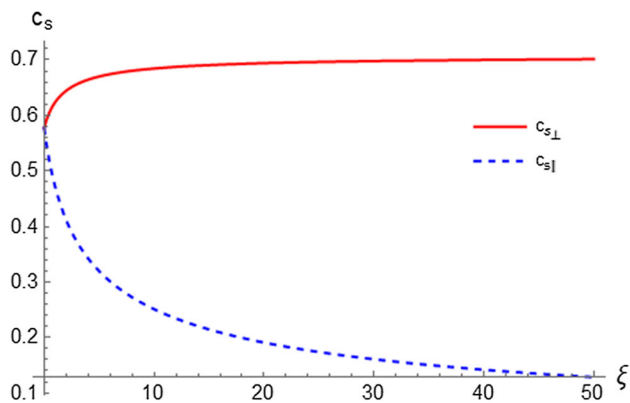


Fig. 2 Plots of the transverse $c_{s\perp}$ (39) (solid) and longitudinal $c_{s\parallel}$ (46) (dashed) speed of sound as functions of the anisotropy parameter ξ in units of the speed of light

while both $\delta_{\perp}(\xi|\sigma)$ and $\rho_{\perp}(\xi)$ grow with ξ , their longitudinal counterparts $\delta_{\parallel}(\xi|\sigma)$ and $\rho_{\parallel}(\xi)$ decay with increasing anisotropy.

From Fig. 1 we see that starting from the same (negative) value δ_{iso} at $\xi = 0$, the relative velocity drop $\delta_{\perp}(\xi|\sigma)$ grows with ξ towards its asymptotic value given in (42). This means that the velocity gap for the transverse shock wave shrinks with growing ξ so that the transverse shock wave weakens with increasing anisotropy. On the contrary, the relative velocity drop $\delta_{\parallel}(\xi|\sigma)$ decays with ξ towards its asymptotic value given in (49) with, therefore, the relative velocity gap for the longitudinal shock wave widening with growing ξ so that the longitudinal shock wave strengthens with increasing anisotropy. At asymptotically large anisotropies $\xi \rightarrow \infty$ the gap between the transverse and longitudinal relative velocity drop reaches

$$(\delta_{\perp}(\xi|\sigma) - \delta_{\parallel}(\xi|\sigma))\Big|_{\xi \rightarrow \infty} \rightarrow \frac{(\sigma - 1)^2}{\sigma(2\sigma + 1)} \quad (50)$$

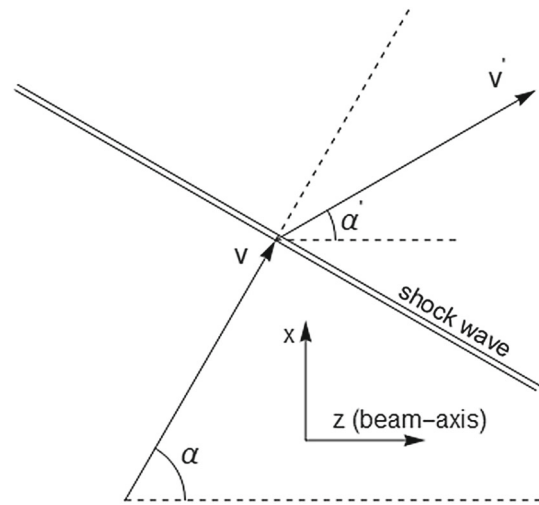


Fig. 3 Transformation of flow velocity by the shock wave front. Upstream flow moves with velocity v at an angle α to the direction of anisotropy (beam axis) and downstream flow moves with velocity v' at an angle α' to the beam axis

As to the anisotropy behaviour of the velocities product or, equivalently, the corresponding speed of sound squared, from Fig. 2 we see that the transverse speed of sound $c_{s\perp}$ grows from $1/\sqrt{3}$ at $\xi = 0$ to $1/\sqrt{2}$ at $\xi \rightarrow \infty$ while the longitudinal one $c_{s\parallel}$ decays from the same value $1/\sqrt{3}$ at $\xi = 0$ to 0 at $\xi \rightarrow \infty$. Since the existence of a shock wave is possible only when the flow moves with a velocity greater than the speed of sound, a much lower flow velocity is required for the shock wave generation in the direction of anisotropy. Therefore, for larger anisotropies formation of longitudinal shock waves is becomes progressively easier while that of transverse ones is, on the contrary, becoming more difficult.

2.4 Normal shock wave at an arbitrary polar angle

In this section we develop a description of a normal shock wave incident at an arbitrary angle with respect to the anisotropy direction, i.e. in the considered case to the z (beam) axis. A major new element we are going to encounter is that, in contrast with the above-considered cases of transverse and longitudinal shock waves, in this case a transformation $\mathbf{v} \rightarrow \mathbf{v}'$ of the upstream velocity \mathbf{v} to the downstream one \mathbf{v}' involves changes both in the absolute value of the flow velocity and the direction of its propagation, see Fig. 3.

To characterise the transformation $\mathbf{v} \rightarrow \mathbf{v}'$ we introduce the following variables describing changes in the absolute value and direction of flow velocity across the shock wave front:

$$\delta_{\alpha\alpha'}(\xi) = \frac{|\mathbf{v}'(\xi|\alpha)| - |\mathbf{v}(\xi|\alpha')|}{|\mathbf{v}(\xi|\alpha)|}, \quad \beta(\xi) = \alpha'(\xi) - \alpha \quad (51)$$

where $\delta_{\alpha\alpha'}(\xi)$ generalises the variables $\delta_{\perp}(\xi\sigma)$ and $\delta_{\parallel}(\xi\sigma)$ defined in (39) and (46) correspondingly¹.

2.4.1 General equations

Let us consider a flow moving at an angle α to the direction of the beam axis (Fig. 3). To simplify formulae due to the symmetry in the Oxy plane one can consider flow propagation in the Oxz plane. Let us express U_{μ} and Z_{μ} through longitudinal rapidity ϑ

$$U_{\mu} = (u_0 \cosh \vartheta, u_x, 0, u_0 \sinh \vartheta), \tag{52}$$

$$Z_{\mu} = (\sinh \vartheta, 0, 0, \cosh \vartheta), \tag{53}$$

introduce transverse rapidities γ, γ' by

$$u_x = \sinh \gamma, \quad u_0 = \cosh \gamma, \tag{54}$$

$$u'_x = \sinh \gamma', \quad u'_0 = \cosh \gamma' \tag{55}$$

and denote the difference between angles α' and α denote as β . The corresponding formulae for the components of flow velocity read

$$\begin{aligned} v_x &= \frac{u_x}{u_0} = \frac{\tanh \gamma}{\cosh \vartheta} = v \cos \alpha, \\ v_z &= \frac{u_z}{u_0} = \tanh \vartheta = v \sin \alpha, \end{aligned} \tag{56}$$

$$\begin{aligned} v'_x &= \frac{u'_x}{u'_0} = \frac{\tanh \gamma'}{\cosh \vartheta'} = v' \cos \alpha', \\ v'_z &= \frac{u'_z}{u'_0} = \tanh \vartheta' = v' \sin \alpha'. \end{aligned} \tag{57}$$

From Eqs. (56, 57) one gets the following expressions for ϑ, ϑ' :

$$\begin{aligned} \vartheta &= \operatorname{arctanh} [\tanh \gamma \tan \alpha], \\ \vartheta' &= \operatorname{arctanh} [\tanh \gamma' \tan \alpha']. \end{aligned} \tag{58}$$

Let us choose the following parametrisation for the components of the vector normal to the discontinuity surface:

$$N_{\mu} = (0, \sin \alpha, 0, \cos \alpha). \tag{59}$$

With the parametrisation (59) the matching conditions (2) take the following form:

$$\begin{aligned} &-(3P_{\perp} + P_{\parallel}) \cosh \gamma \cosh \vartheta \\ &(\sinh \gamma \cos \alpha + \cosh \gamma \sinh \vartheta \sin \alpha) \\ &+ (3P'_{\perp} + P'_{\parallel}) \cosh \gamma' \cosh \vartheta' \end{aligned}$$

$$\begin{aligned} &(\sinh \gamma' \cos \alpha + \cosh \gamma' \sinh \vartheta' \sin \alpha) \\ &+ (P_{\perp} - P_{\parallel}) \sinh \vartheta \cosh \vartheta \sin \alpha \\ &-(P'_{\perp} - P'_{\parallel}) \sinh \vartheta' \cosh \vartheta' \sin \alpha = 0, \end{aligned} \tag{60}$$

$$\begin{aligned} &-(3P_{\perp} + P_{\parallel}) \cosh \gamma \sinh \vartheta \\ &(\sinh \gamma \cos \alpha + \cosh \gamma \sinh \vartheta \sin \alpha) - P_{\perp} \sin \alpha \\ &+ (3P'_{\perp} + P'_{\parallel}) \cosh \gamma' \sinh \vartheta' \\ &(\sinh \gamma' \cos \alpha + \cosh \gamma' \sinh \vartheta' \sin \alpha) + P'_{\perp} \sin \alpha \\ &+ (P_{\perp} - P_{\parallel}) \cosh \vartheta \cosh \vartheta \sin \alpha \\ &-(P'_{\perp} - P'_{\parallel}) \cosh \vartheta' \cosh \vartheta' \sin \alpha = 0, \end{aligned} \tag{61}$$

$$\begin{aligned} &-(3P_{\perp} + P_{\parallel}) \sinh \gamma (\sinh \gamma \cos \alpha + \cosh \gamma \sinh \eta \sin \alpha) \\ &- P_{\perp} \cos \alpha \\ &+ (3P'_{\perp} + P'_{\parallel}) \sinh \gamma' (\sinh \gamma' \cos \alpha + \cosh \gamma' \sinh \vartheta' \sin \alpha) \\ &+ P'_{\perp} \cos \alpha = 0, \end{aligned} \tag{62}$$

The Eqs. (60)–(62) constitute a system of equations for three unknowns γ, γ', α' that depend on three parameters σ, ξ, α that is solved numerically. The formulae (56, 57) then translate a solution for γ, γ', α' into vectors of upstream and downstream velocities.

2.4.2 Flow deflection by the shock wave front

In isotropic relativistic hydrodynamics, a normal shock wave changes only the absolute value of the incident flow velocity, but not the direction of the flow passing through it. Our analysis of transverse and longitudinal normal shock waves in Sects. 2.3.1 and 2.3.2 has shown that in these cases deflection of the incident flow is absent in anisotropic hydrodynamics as well. However, it turns out that this is no longer true for normal shock waves incident at an arbitrary polar angle. In this case the flow is deflected by the shock wave front so that in notations of Fig. 3 one has $\alpha' \neq \alpha$.

In Fig. 4 we plot the deflection angle $\beta = \alpha' - \alpha$ as a function of the incidence angle α for several values of σ and anisotropy parameter ξ . In all the cases the function $\beta(\alpha)$ takes negative values and has a minimum at some α^* . At fixed ξ the depth of this minimum grows with σ . At fixed σ with growing ξ the minimum a) gets deeper and b) its position shifts towards smaller α . Let us note that for strong anisotropy, large σ and incidence angles $\alpha \leq \pi/4$ we have flow deviation from the initial direction by almost $\pi/2$ so that the upstream flow tends to propagate along the shock wave front.

Let us note that from the bottom plots of Fig. 4 we see that for large anisotropies one observes a rapid change of regimes indicating an existence of effective instability at small angles α .

¹ To avoid overloaded notation in this paragraph we do not explicitly indicate the σ dependence of quantities like $\delta_{\alpha\alpha'}(\xi)$.

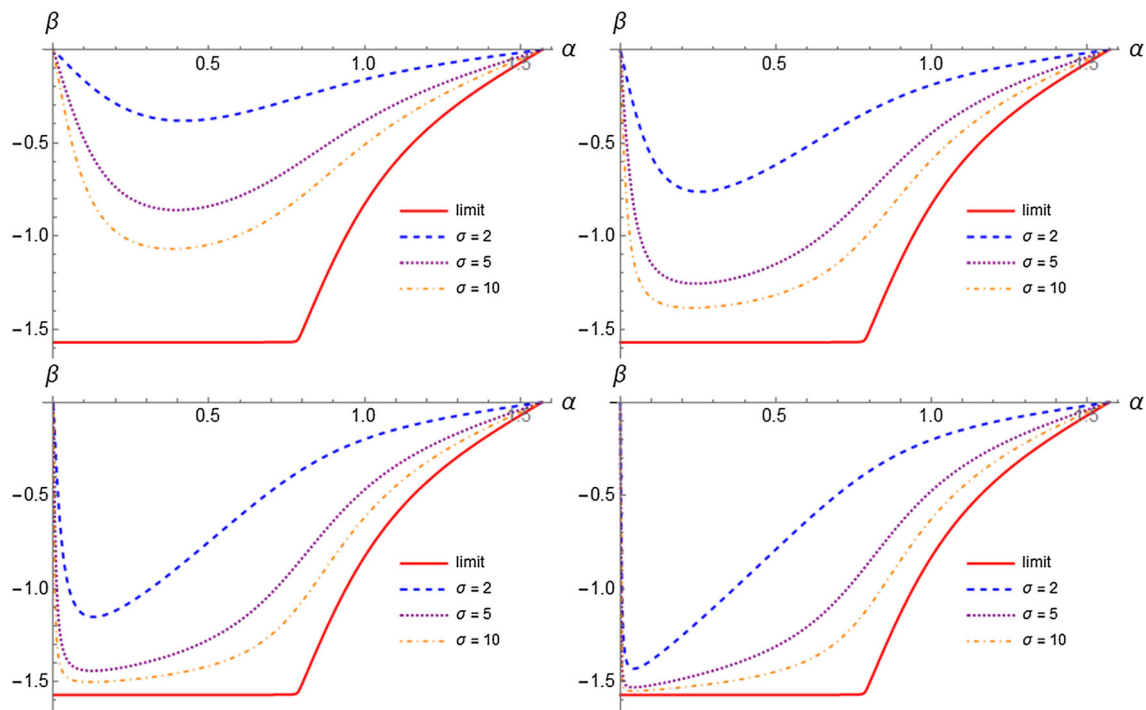


Fig. 4 Plot of the deflection angle $\beta = \alpha' - \alpha$ as a function of the initial angle α for $\sigma = 2$ (dashed line), $\sigma = 5$ (dotted line) and $\sigma = 10$ (dash-dotted line) for $\xi = 5$ (top left), $\xi = 20$ (top right), $\xi = 100$ (bottom left), $\xi = 1000$ (bottom right). Each plot contains the limiting curve $\sigma \rightarrow \infty, \xi \rightarrow \infty$ (solid line)

2.4.3 Transformation $|\mathbf{v}(\xi)| \rightarrow |\mathbf{v}'(\xi)|$

To characterise the transformation $|\mathbf{v}(\xi)| \rightarrow |\mathbf{v}'(\xi)|$ let us first consider the anisotropy dependence of the absolute value of upstream velocity $v_\alpha(\xi) \equiv |\mathbf{v}(\xi|\alpha)|$ at different incidence angles $\alpha, \alpha \in [0, \pi/2]$. The resulting curves are shown in Fig. 5 for two different values of σ .

From Fig. 5 we see, for both values of σ , a transition from convex decaying $v_\alpha(\xi)$ at small incidence angles α to concave growing pattern at large incidence angles. The transition between the two patterns takes place at $\alpha_{crit} \sim \pi/4$.

Second, let us analyse the anisotropy dependence of the absolute value of downstream velocity $v'_\alpha(\xi) \equiv |\mathbf{v}'(\xi|\alpha)|$ at different incidence angles $\alpha, \alpha \in [0, \pi/2]$. The resulting curves are shown in Fig. 6 for the same values of σ as in Fig. 5.

The behaviour of $v'_\alpha(\xi)$ is characterised by two different patterns. The transition between them, similarly to the above-considered case of upstream velocity, also takes place at $\alpha_{crit} \sim \pi/4$:

- In the interval of incidence angles $\alpha \in (0, \pi/4)$ a growth at large anisotropies is preceded by the minimum at some $\xi^*(\alpha)$ such that $\xi^*(\alpha) \rightarrow 0$ at $\alpha \rightarrow \alpha_{crit}$ and $\xi^*(\alpha) \rightarrow \infty$ at $\alpha \rightarrow 0$. A detailed illustration of this pattern is presented in Fig. 7.

- In the interval of incidence angles $\alpha \in (\pi/4, \pi/2)$, similarly to the behaviour of $v_\alpha(\xi)$ in the same interval of angles, the function $v'_\alpha(\xi)$ is a concave growing one smoothly approaching the limiting curve for the transverse shock wave at $\alpha = \pi/2$;

Let us note that at small angles the form of $v'_\alpha(\xi)$ is extremely sensitive to the value of α , see Fig. 8, possibly indicating an unstable velocity transformation pattern of the “almost longitudinal” shock waves.

2.4.4 Transformation $|\mathbf{v}| \rightarrow |\mathbf{v}'|$: angular dependence

Let us start our analysis of the angular dependence of velocity transformation $|\mathbf{v}| \rightarrow |\mathbf{v}'|$ with studying the angular dependence of the pattern of anisotropy dependence of the relative change of the absolute value of velocity $\delta_{\alpha\alpha'}(\xi)$ defined in Eq. (51) induced by a superposition of the corresponding patterns for $|\mathbf{v}(\xi|\alpha)|$ and $|\mathbf{v}'(\xi|\alpha)|$ studied in the previous paragraph 2.4.3.

As seen at Fig. 9, for each shock wave incidence angle $\alpha \in (0, \pi/2)$ at some critical anisotropy $\xi^*(\alpha)$ the relative velocity drop $\delta_{\alpha\alpha'}(\xi)$ changes its sign. This means that at sufficiently large anisotropies the rarefaction shock wave pattern with $\delta_{\alpha\alpha'}(\xi) < 0$ turns into the compression shock wave one with $\delta_{\alpha\alpha'}(\xi) > 0$ corresponding to acceleration of the flow by the shock wave so that we see a dramatic anisotropy-induced

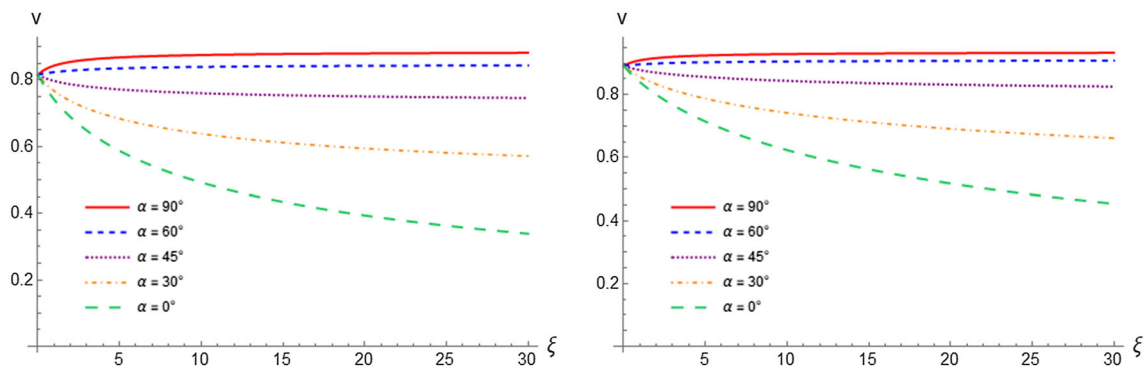


Fig. 5 Plots of the absolute value of upstream velocity $|v(\xi|\alpha)|$ as a function of the anisotropy parameter ξ for $\alpha = \pi/2$ (solid), $\alpha = 2\pi/3$ (dashed), $\alpha = \pi/4$ (dotted), $\alpha = \pi/6$ (dash-dotted) and $\alpha = 0$ (long dash) for $\sigma = 5$ (left) and $\sigma = 10$ (right)

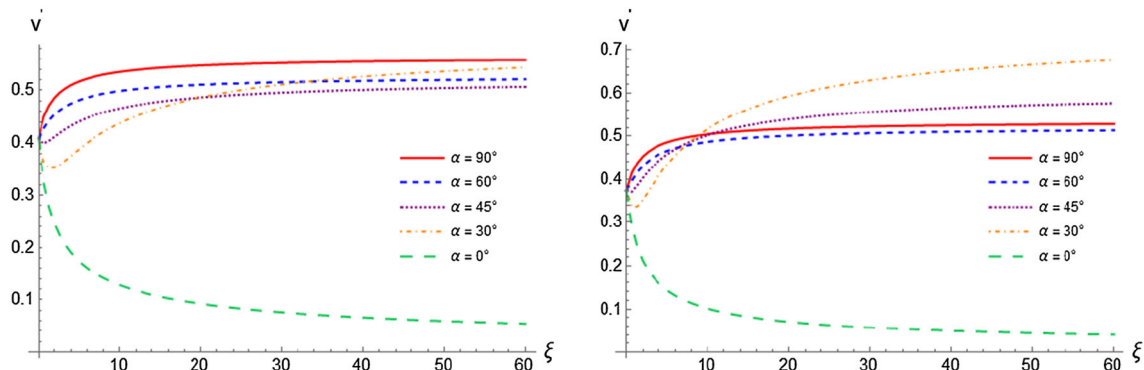


Fig. 6 Plots of the absolute value of downstream velocity $|v'(\xi|\alpha)|$ as a function of the anisotropy parameter ξ for $\alpha = \pi/2$ (solid), $\alpha = 2\pi/3$ (dashed), $\alpha = \pi/4$ (dotted), $\alpha = \pi/6$ (dash-dotted) and $\alpha = 0$ (long dash) for $\sigma = 5$ (left) and $\sigma = 10$ (right)

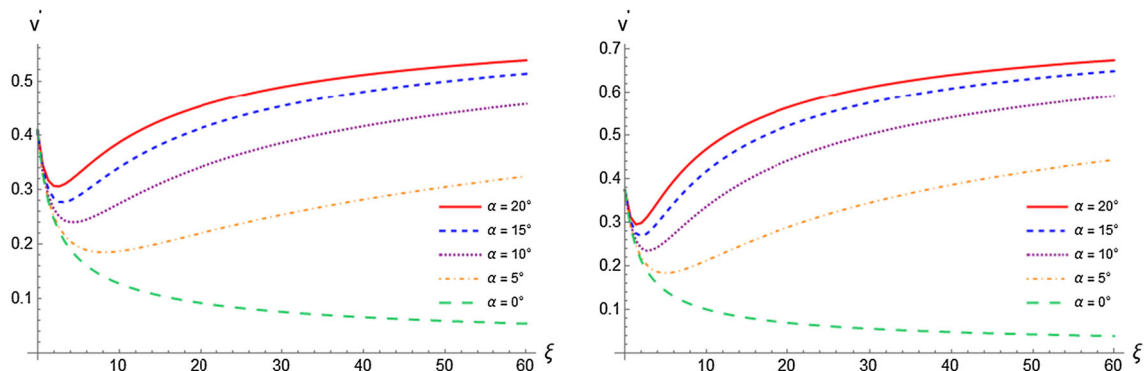


Fig. 7 Plots of the absolute value of downstream velocity $|v'(\xi|\alpha)|$ as a function of the anisotropy parameter ξ for $\alpha = 20^\circ$ (solid), $\alpha = 15^\circ$ (dashed), $\alpha = 10^\circ$ (dotted), $\alpha = 5^\circ$ (dash-dotted) and $\alpha = 0$ (long dash) for $\sigma = 5$ (left) and $\sigma = 10$ (right)

transition in the very nature of shock waves in anisotropic relativistic hydrodynamics.

Let us now turn to the analysis the relative change of the absolute value of velocity $\delta_{\alpha\alpha'}(\xi)$ as a function of the incidence angle α at fixed ξ . In Figs. 10, 11 we plot this dependence for several relatively small (Fig. 10) and very large (Fig. 11) values of the anisotropy parameter and four different values of σ in Fig. 10 and $\sigma = 100$ in Fig. 11.

From Figs. 10, 10 we see that the superposition of the angular dependencies of $|v(\xi|\alpha)|$ and $|v'(\xi|\alpha)|$ leads to a hump-backed pattern for $\delta_{\alpha\alpha'}(\xi)$ with the hump moving from large to small angles and becoming more pronounced with increasing anisotropy.

For large σ and ξ there appears an interval of angles in which $\delta_{\alpha\alpha'}(\xi)$ changes its sign and, therefore, a shock wave pattern changes from the rarefaction to the compression one. The width of this interval grows with σ .

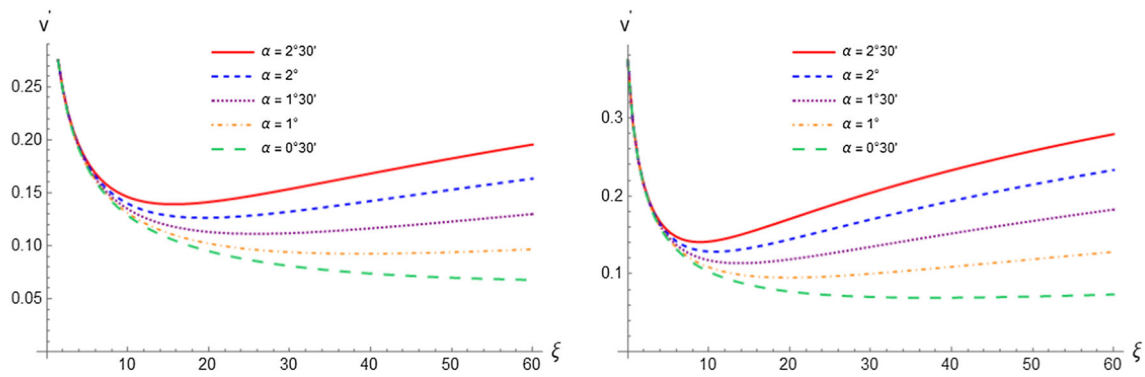


Fig. 8 Plots of the absolute value of downstream velocity $|v'(\xi|\alpha)|$ as a function of the anisotropy parameter ξ for small incidence angles $\alpha = 2^\circ 30'$ (solid), $\alpha = 2^\circ$ (dashed), $\alpha = 1^\circ 30'$ (dotted), $\alpha = 1^\circ$ (dash-dotted) and $\alpha = 0^\circ 30'$ (long dash) for $\sigma = 5$ (left) and $\sigma = 10$ (right)

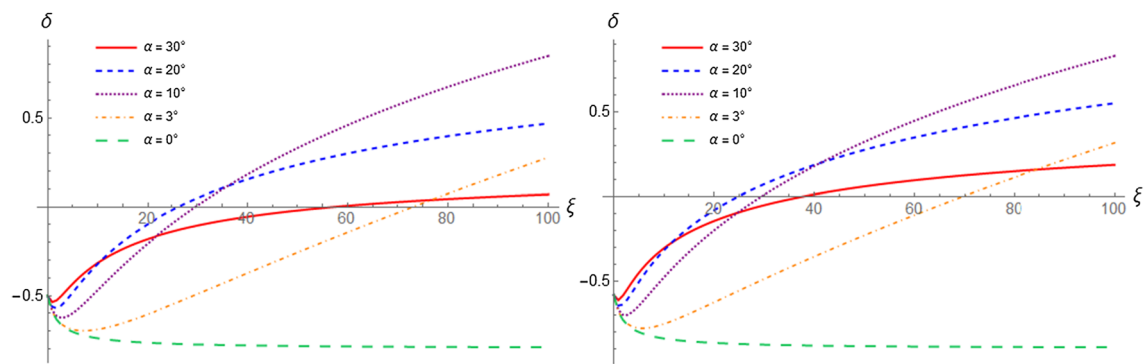


Fig. 9 Plots of the relative change of the absolute value of velocity $\delta_{\alpha\alpha'}(\xi)$ as a function of anisotropy parameter for $\alpha = 30^\circ$ (solid), $\alpha = 20^\circ$ (dashed), $\alpha = 10^\circ$ (dotted), $\alpha = 3^\circ$ (dash-dotted) and $\alpha = 0$ (long dash) for $\sigma = 5$ (left) and $\sigma = 10$ (right)

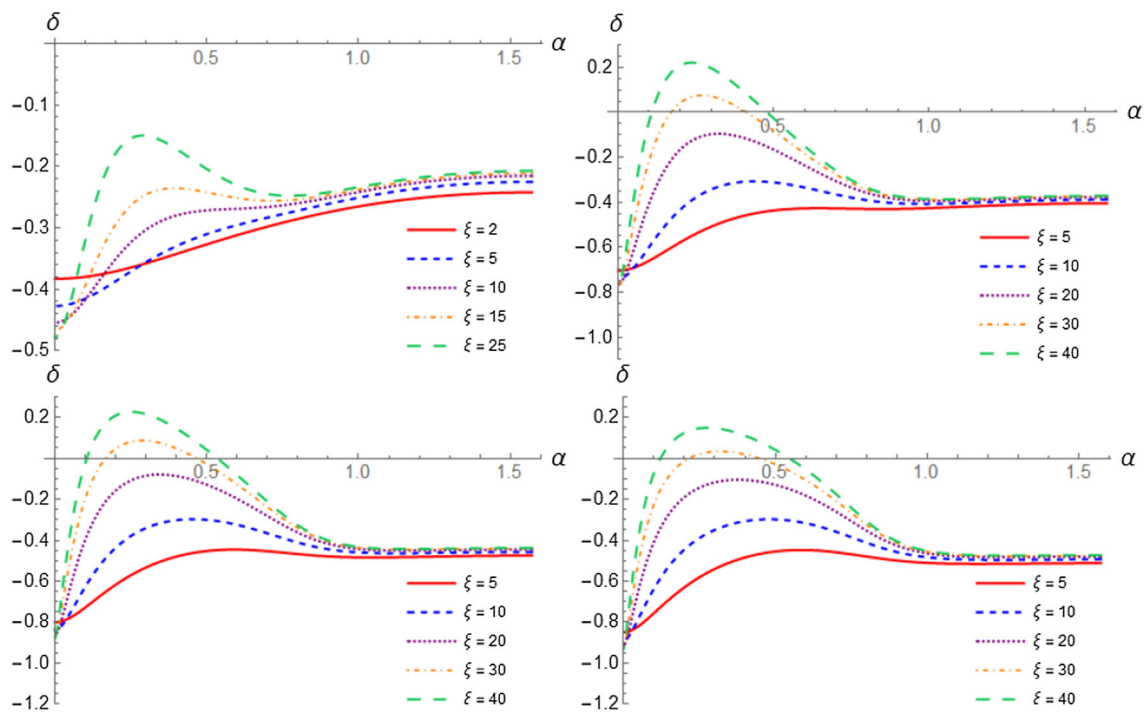


Fig. 10 Plots of the relative change of the absolute value of velocity $\delta_{\alpha\alpha'}(\xi) < 0$ as a function of the incidence angle α for $\xi = 2$ (solid), $\xi = 5$ (dashed), $\xi = 10$ (dotted), $\xi = 15$ (dash-dotted) and $\xi = 25$ (long dash) for $\sigma = 2$ (top left), $\sigma = 5$ (top right), $\sigma = 10$ (bottom left) and $\sigma = 20$ (bottom right)

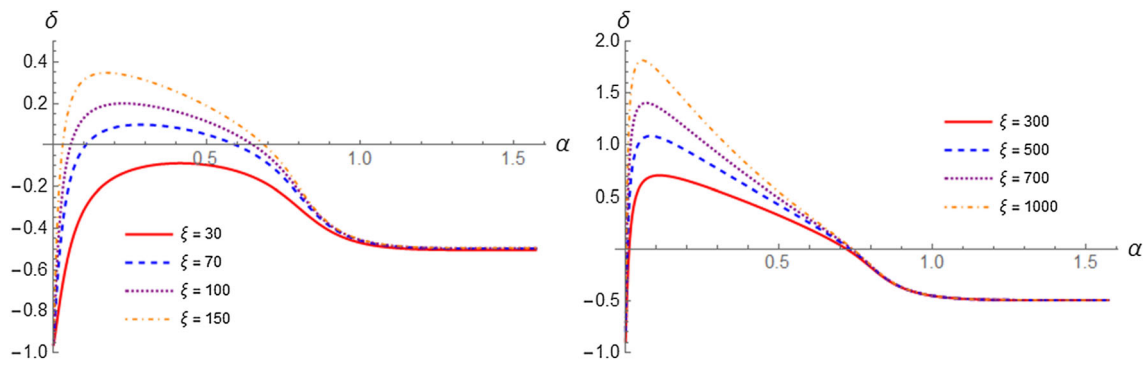


Fig. 11 Plots of the relative change of the absolute value of velocity $\delta_{\alpha\alpha'}(\xi)$ as a function of the incidence angle α for large values of the anisotropy parameter $\xi = 30$ (solid), $\xi = 70$ (dashed), $\xi = 100$ (dotted) and $\xi = 150$ (dash-dotted)

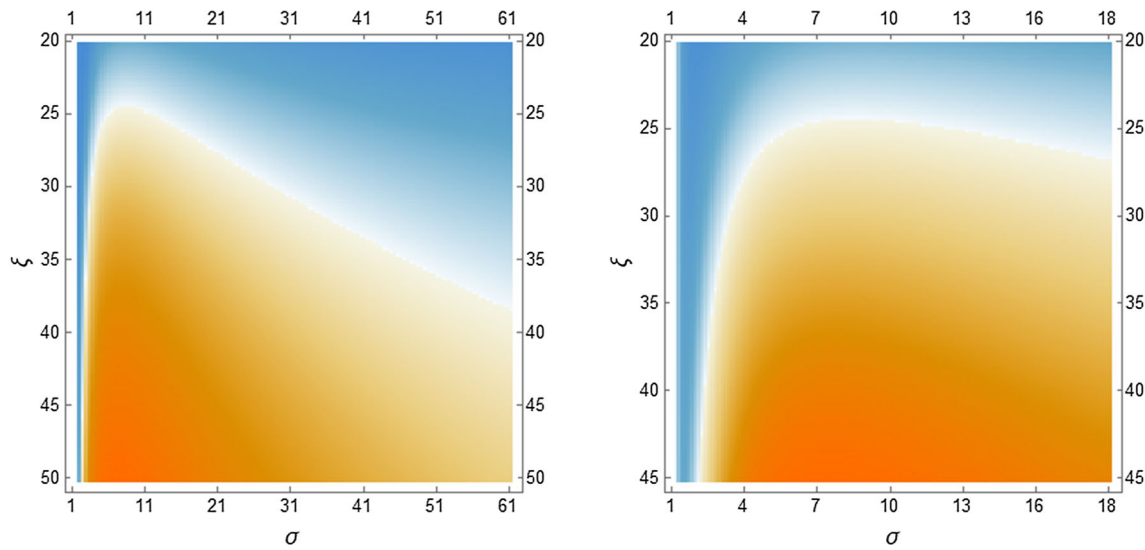


Fig. 12 Plot of the location of the maximum of the relative change of the absolute value of velocity $\delta_{\alpha\alpha'}(\xi)$. Warmer tones correspond to its positive values and colder tones to the negative ones. White color

corresponds to the values close to zero. For large anisotropies the white band defines three types of shock waves: weak shock wave, shock wave with deceleration of the flow, strong shock wave

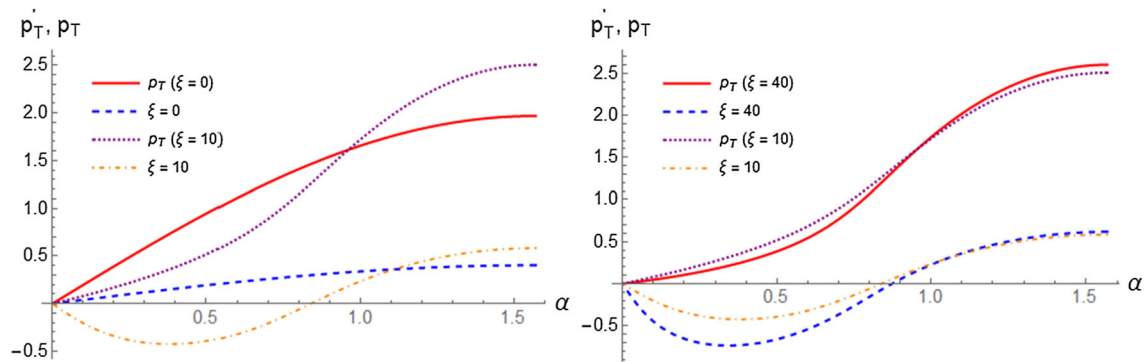


Fig. 13 Left: plots of the anisotropy dependence of the transverse momentum $p_T(\alpha|\xi)$ for $\xi = 0$ (solid), $\xi = 10$ (dotted) and $p'_T(\alpha|\xi)$ for $\xi = 0$ (dashed), $\xi = 10$ (dash-dotted). Right: plots of the anisotropy

dependence of the transverse momentum $p_T(\alpha|\xi)$ for $\xi = 40$ (solid), $\xi = 10$ (dotted) and $p'_T(\alpha|\xi)$ for $\xi = 40$ (dashed), $\xi = 10$ (dash-dotted)

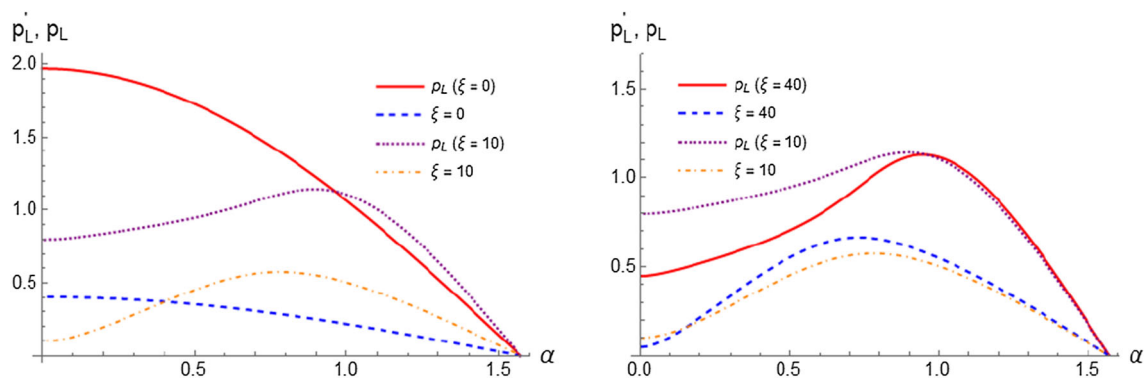


Fig. 14 Left: plots of the anisotropy dependence of the longitudinal momentum $p_L(\alpha|\xi)$ for $\xi = 0$ (solid), $\xi = 10$ (dotted) and $p'_L(\alpha|\xi)$ for $\xi = 0$ (dashed), $\xi = 10$ (dashed-dotted). Right: plots of the anisotropy

dependence of the longitudinal momentum $p_L(\alpha|\xi)$ for $\xi = 40$ (solid), $\xi = 10$ (dotted) and $p'_L(\alpha|\xi)$ for $\xi = 40$ (dashed), $\xi = 10$ (dashed-dotted)

In Fig. 12 we plot a position of the hump in the (ξ, σ) plane.

From Fig. 12 we see that $\delta(\alpha)$ touches zero for two values of σ . For small σ and ξ the dependence is nonlinear. For anisotropy parameters ξ below a certain value, as σ grows, δ does twice undergo a transition between negative and positive values. Thus, for such values of ξ , there are two possible types of shock waves with a feature typical for compression shock waves - a deceleration of the upstream flow. The first type of waves is characterised by small values of σ while for the second type σ takes large values that grow almost linearly with increasing ξ .

2.4.5 Transformation $(p_T, p_L) \rightarrow (p'_T, p'_L)$: angular dependence

Of particular interest for describing the effects of the downstream and upstream flows related to shock wave formation for heavy ion collisions are the associated transverse and longitudinal momenta that contribute to transverse momentum and rapidity spectra. For a shock wave incident at polar angle α the corresponding transverse and longitudinal momenta for the upstream flow read

$$p_T = p \sin \alpha, \quad p_L = p \cos \alpha. \tag{63}$$

Analogous formulae hold for the downstream flow. The resulting angular dependencies $p_T(\alpha|\xi)$, $p'_T(\alpha|\xi)$, $p_L(\alpha|\xi)$ and $p'_L(\alpha|\xi)$ are shown, for several values of ξ , in Figs. 13 and 14 correspondingly.

We see from Fig. 13 that in comparison to isotropic production there takes place a reversion of p'_T at small incidence angles $\alpha < \alpha^*_T(\xi)$ and more p'_T is produced at large incidence angles $\alpha^*_T(\xi) < \alpha < \pi/2$ where $\alpha^*_T(\xi)$ is an anisotropy - dependent scale separating the regimes of transverse momentum reversal at small α and its enrichment at large α .

As to the longitudinal momenta, in Fig. 13 we observe, in comparison to the isotropic case, a pattern of depletion of longitudinal momentum at small angles $\alpha < \alpha^*_L(\xi)$ and its enhancement at large angles $\alpha^*_L(\xi) < \alpha < \pi/2$ where $\alpha^*_L(\xi)$ is a regime-dividing scale *different* from its transverse counterpart $\alpha^*_T(\xi)$.

3 Conclusions

Let us summarise the main results obtained in the paper:

- General equations describing shock waves in relativistic anisotropic hydrodynamics were derived.
- In distinction with the second order viscous relativistic hydrodynamics these equations are valid for arbitrarily strong shock waves.
- Solutions describing normal shock waves incident at an arbitrary angle with respect to collision axis as well as transverse and longitudinal shock waves were obtained and compared with the corresponding results for the isotropic case.
- A new phenomenon of anisotropy - related angular deflection of the upstream flow was described.
- Transformation of velocities and momenta by the shock wave front was analysed.

In our view among the problems worth further studies the most interesting and pressing one is an analysis of entropy transformation by the shock wave front in relativistic anisotropic hydrodynamics. It is well known that anisotropy gives rise to a new source of entropy production in anisotropic hydrodynamics so it is very interesting to see how the standard pattern of entropy production by shock waves in isotropic hydrodynamics changes in the anisotropic case. We plan to address this problem in the near future.

Acknowledgements The work was supported by the RFBR Grant 18-02-40069.

Data Availability Statement This manuscript has no associated data or the data will not be deposited. [Authors’ comment: The paper is purely theoretical, there is no data associated with it.]

Declarations

Conflict of interest The authors have no conflicts of interest to declare that are relevant to the content of this article.

Open Access This article is licensed under a Creative Commons Attribution 4.0 International License, which permits use, sharing, adaptation, distribution and reproduction in any medium or format, as long as you give appropriate credit to the original author(s) and the source, provide a link to the Creative Commons licence, and indicate if changes were made. The images or other third party material in this article are included in the article’s Creative Commons licence, unless indicated otherwise in a credit line to the material. If material is not included in the article’s Creative Commons licence and your intended use is not permitted by statutory regulation or exceeds the permitted use, you will need to obtain permission directly from the copyright holder. To view a copy of this licence, visit <http://creativecommons.org/licenses/by/4.0/>.

Funded by SCOAP³.

Appendix A: Subluminality condition for shock waves in relativistic anisotropic hydrodynamics

In the anisotropic case the necessary subluminality condition $N^\mu N_\mu < 0$ for the four-vector N_μ orthogonal to the discontinuity surface can be studied by writing the corresponding equations generalising Eqs. (5, 6) for the isotropic case.

From the matching conditions (2) and the expression (20) for the energy momentum tensor one gets the following system of equations:

$$\text{Det } \Lambda = \begin{vmatrix} 0 & -(3P'_\perp + P'_\parallel)B & (P'_\perp - P_\parallel) & (P'_\perp - P'_\parallel)D \\ -(3P_\perp + P_\parallel)C & 0 & (P_\perp - P_\parallel)D & (P_\perp - P'_\parallel) \\ (2P_\perp + P_\parallel + P'_\perp) & -(3P'_\perp + P'_\parallel)A & 0 & (P'_\perp - P'_\parallel)C \\ -(3P_\perp + P_\parallel)A & (2P'_\perp + P'_\parallel + P_\perp) & (P_\perp - P_\parallel)B & 0 \end{vmatrix} = 0. \tag{75}$$

$$(\varepsilon + P'_\perp)x = (\varepsilon' + P'_\perp)Ax' - (P'_\perp - P'_\parallel)Cy', \tag{64}$$

$$(\varepsilon' + P_\perp)x' = (\varepsilon + P_\perp)Ax - (P_\perp - P_\parallel)By, \tag{65}$$

$$(P'_\perp - P_\parallel)y = (\varepsilon' + P'_\perp)Bx' - (P'_\perp - P'_\parallel)Dy', \tag{66}$$

$$(P_\perp - P'_\parallel)y' = (\varepsilon + P_\perp)Cx - (P_\perp - P_\parallel)Dy, \tag{67}$$

where

$$x = U_\mu N^\mu, \quad x' = U'_\mu N^\mu, \quad A = U'_\mu U^\mu, \quad B = U'_\mu Z^\mu, \tag{68}$$

$$y = Z_\mu N^\mu, \quad y' = Z'_\mu N^\mu, \quad C = Z'_\mu U^\mu, \quad D = Z'_\mu Z^\mu. \tag{69}$$

In ultra-relativistic case we have

$$(2P_\perp + P_\parallel + P'_\perp)x = (3P'_\perp + P'_\parallel)Ax' - (P'_\perp - P'_\parallel)Cy', \tag{70}$$

$$(2P'_\perp + P'_\parallel + P_\perp)x' = (3P_\perp + P_\parallel)Ax - (P_\perp - P_\parallel)By, \tag{71}$$

$$(P'_\perp - P_\parallel)y = (3P'_\perp + P'_\parallel)Bx' - (P'_\perp - P'_\parallel)Dy', \tag{72}$$

$$(P_\perp - P'_\parallel)y' = (3P_\perp + P_\parallel)Cx - (P_\perp - P_\parallel)Dy, \tag{73}$$

Our purpose is to evaluate the sign of $N_\mu N^\mu$ for check subluminality condition, which is $N^\mu N_\mu < 0$. Using the matching conditions (2) one can find

$$N_\mu N^\mu = \frac{1}{P_\perp - P'_\perp} \left[(3P_\perp + P_\parallel)x^2 - (3P'_\perp + P'_\parallel)x'^2 - (P_\perp - P_\parallel)y^2 + (P'_\perp - P'_\parallel)y'^2 \right]. \tag{74}$$

The system of Eqs. (70–73) has solutions if the condition for the determinant is satisfied.

It is worth saying that in the borderline cases, then the flow moves along the axes Ox and Oz , the equation $\text{Det } \Lambda = 0$ gives the correct solutions for Δ , which agree with solutions for the velocities in anisotropic case.

Then, solving the system of equations, we can express x', y, y' through x , that give us

$$N_\mu N^\mu = \frac{1}{P_\perp - P'_\perp} \Phi(P_\perp, P_\parallel, P'_\perp, P'_\parallel, A, B, C, D)x^2 \tag{76}$$

Using Eqs. (52,53) and (54,55) we get the following expressions for A , B , C and D :

$$A = U'_\mu U^\mu = \cosh \gamma \cosh \gamma' \cosh(\vartheta - \vartheta') - \sinh \gamma \sinh \gamma' \tag{77}$$

$$B = U'_\mu Z^\mu = \cosh \gamma' \sinh(\vartheta - \vartheta'), \tag{78}$$

$$C = Z'_\mu U^\mu = -\cosh \gamma \sinh(\vartheta - \vartheta') \tag{79}$$

$$D = Z'_\mu Z^\mu = -\cosh(\vartheta - \vartheta'). \tag{80}$$

Thus, the system of equations will explicitly depend only on the difference $\vartheta - \vartheta'$, and not on the values themselves. Let's denote $\Delta = \vartheta - \vartheta'$.

Due to the anisotropic hydrodynamic P_\perp , P_\parallel are divided into anisotropic and isotropic parts according to the formulas (13, 14). Also denote $\sigma = P'_{iso}/P_{iso}$. From the equation $\text{Det } \Lambda = 0$ we can get the value Δ . Thus, we have 4 unknowns $\sigma, \xi, \gamma, \gamma'$, of which σ, ξ are the parameters of the system. Also, solving the equation $\text{Det } \Lambda = 0$ allow us to obtain a consistent system of Eqs. (70–73), so it is possible to choose one among the values x, x', y, y' , and express others through it. Let, for example, this be the value x , then, from the expression (74), we can write

$$N_\mu N^\mu = \frac{1}{R_\perp(\xi)(1 - \sigma)} \Phi(\sigma, \xi, \gamma, \gamma', \Delta)x^2. \tag{81}$$

One can construct the following function

$$S(\sigma, \xi, \gamma, \gamma') = \text{sign} \left(\frac{1}{R_\perp(\xi)(1 - \sigma)} \Phi(\sigma, \xi, \gamma, \gamma', \Delta(\sigma, \xi, \gamma, \gamma')) \right), \tag{82}$$

that determines the sign of the norm of the vector N^μ .

Denote $T = \tanh \gamma, T' = \tanh \gamma'$ and then he have

$$S(\sigma, \xi, T, T') = \text{sign} \left(\frac{1}{R_\perp(\xi)(1 - \sigma)} \Phi(\sigma, \xi, T, T', \Delta(\sigma, \xi, T, T')) \right), \tag{83}$$

It should be taken into account that the equation $\text{Det } \Lambda = 0$ may not have solutions, then it is convenient to construct the following function:

$$\Omega(\sigma, \xi, T, T') = \begin{cases} -1 & \text{Det } \Lambda = 0 \text{ has no solutions} \\ 0 & S(\sigma, \xi, \gamma, \gamma') = -1 \\ 1 & S(\sigma, \xi, \gamma, \gamma') = 1 \end{cases} \tag{84}$$

As one can see on Fig. 15, it turned out that there is no case of $\Omega = 1$ anywhere. It can also be seen that the graphs show as ξ increases, the region of possible solutions to the

equation $\text{Det } \Lambda = 0$ increases. This fact allows us to assume that in an anisotropic medium, a shock wave can be formed more often than in an isotropic case.

Appendix B

Let us first consider a description of a shock wave propagating perpendicular to the beam axis. Due to the symmetry in Oxy -plane, it sufficient to consider its propagation along the x axis and, correspondingly, choose the following basis:

$$U_\mu = (u_0, u_x, 0, 0), \quad Z_\mu = (0, 0, 0, 1), \tag{85}$$

$$U'_\mu = (u'_0, u'_x, 0, 0), \quad Z'_\mu = Z_\mu = (0, 0, 0, 1). \tag{86}$$

The matching conditions (2) lead to the following system of equations:

$$(\varepsilon + P_\perp)U_0x - P_\perp N_0 - (\varepsilon' + P'_\perp)U'_0x' + P'_\perp N_0 = 0, \tag{87}$$

$$(\varepsilon + P_\perp)U_1x - P_\perp N_1 - (\varepsilon' + P'_\perp)U'_1x' + P'_\perp N_1 = 0, \tag{88}$$

$$-P_\perp N_2 + P'_\perp N_2 = 0, \tag{89}$$

$$-P_\parallel N_3 + P'_\parallel N_3 = 0. \tag{90}$$

The third and fourth equations lead us to the solutions $N_2 = 0$ and $N_3 = 0$. We also take into account the expression for the ultrarelativistic case and obtain

$$(3P_\perp + P_\parallel)u_0(u_0N_0 - u_xN_1) - P_\perp N_0 - (3P'_\perp + P'_\parallel)u'_0(u'_0N_0 - u'_xN_1) + P'_\perp N_0 = 0, \tag{91}$$

$$(3P_\perp + P_\parallel)u_x(u_0N_0 - u_xN_1) - P_\perp N_1 - (3P'_\perp + P'_\parallel)u'_x(u'_0N_0 - u'_xN_1) + P'_\perp N_1 = 0. \tag{92}$$

For the existence of solutions to the remaining two equations on N_0, N_1 , the determinant of the coefficients of the equation should be equal to zero. With introducing the following definitions

$$A_0 = (3P_\perp + P_\parallel)u_0^2 - (3P'_\perp + P'_\parallel)u_0'^2 - (P_\perp - P'_\perp), \tag{93}$$

$$B_0 = -(3P_\perp + P_\parallel)u_0u_x + (3P'_\perp + P'_\parallel)u_0'u'_x, \tag{94}$$

$$A_1 = -B_0 = (3P_\perp + P_\parallel)u_0u_x - (3P'_\perp + P'_\parallel)u_0'u'_x, \tag{95}$$

$$B_1 = -(3P_\perp + P_\parallel)u_x^2 + (3P'_\perp + P'_\parallel)u_x'^2 - (P_\perp - P'_\perp), \tag{96}$$

determinant will take the form

$$\begin{vmatrix} A_0 & B_0 \\ A_1 & B_1 \end{vmatrix} = 0. \tag{97}$$

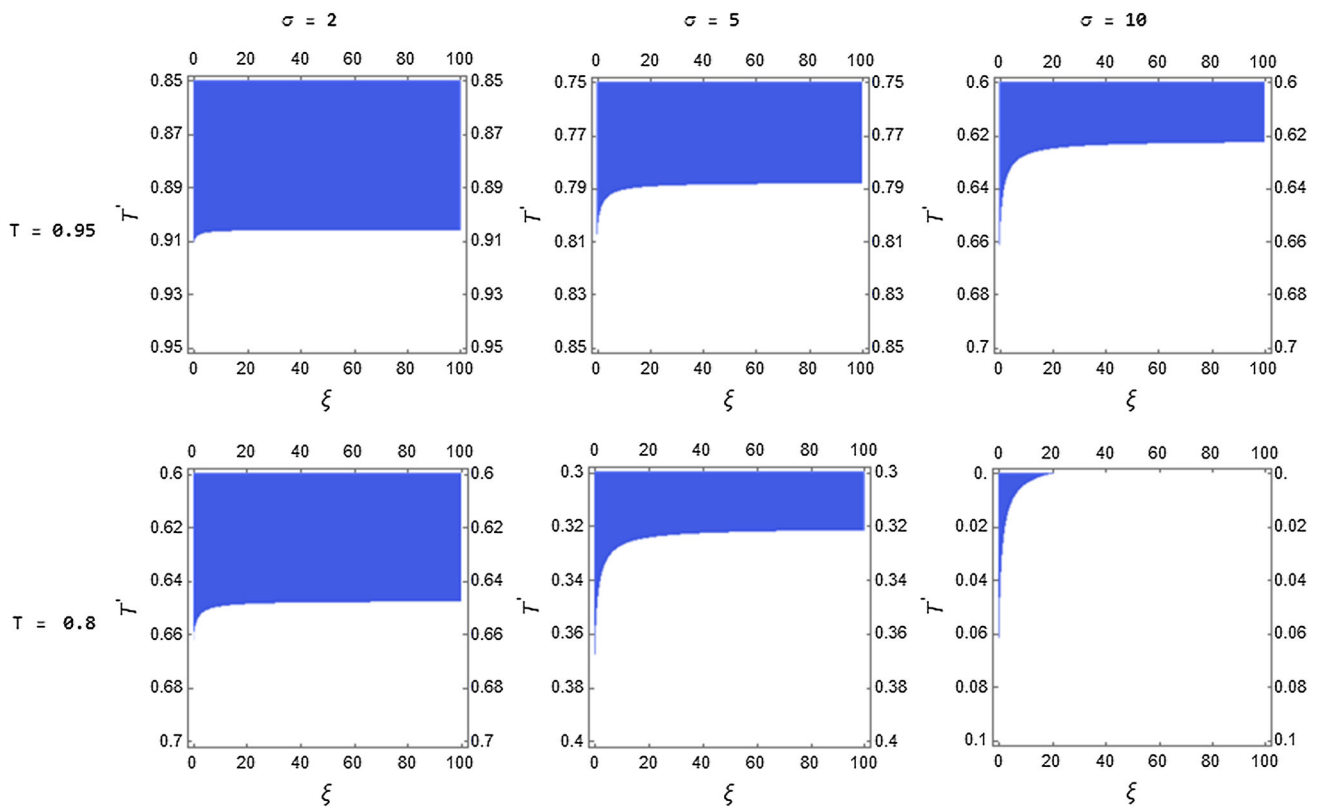


Fig. 15 Plot of $\Omega(\sigma, \xi, T, T')$ as a function of ξ, T' . Blue color denotes $\Omega = -1$, white color - $\Omega = 0$

The one-dimensional formulation of the problem allows us to write expressions for the components of the 4-velocity vector in terms of hyperbolic functions

$$u_x = \sinh \gamma, \quad u_0 = \cosh \gamma, \tag{98}$$

$$u'_x = \sinh \gamma', \quad u'_0 = \cosh \gamma'. \tag{99}$$

Substituting (97) and (93–96) into (97) we obtain

or, more conveniently, as

$$\sinh^2(\gamma - \gamma') = \frac{(2P_{\perp} - P_{\parallel} - 2P'_{\perp} + P'_{\parallel})(P_{\parallel} - P'_{\parallel})}{(3P_{\perp} + P_{\parallel})(3P'_{\perp} + P'_{\parallel})}. \tag{101}$$

In the limit $\xi \rightarrow 0$ the formula above is equal to the solution in the isotropic case [15]. Space-like nature of the normal vector N^{μ} , i.e $N^{\mu}N_{\mu} = -1$, lead to a closed system of equations for N_0, N_1 , solutions of whose are

$$N_0 = \frac{1}{2} \frac{(3P_{\perp} + P_{\parallel}) \cosh(2\gamma - 2\gamma') - (P'_{\parallel} + P_{\perp} + 2P'_{\perp}) \cosh \gamma'}{\sqrt{(P_{\parallel} + 2P_{\perp} + P'_{\perp})^2 \sinh^2(\gamma - \gamma') - (P_{\parallel} - P'_{\parallel})^2 \cosh^2(\gamma - \gamma')}}}, \tag{102}$$

$$N_1 = \frac{1}{2} \frac{(3P_{\perp} + P_{\parallel}) \sinh(2\gamma - 2\gamma') - (P'_{\parallel} + P_{\perp} + 2P'_{\perp}) \sinh \gamma'}{\sqrt{(P_{\parallel} + 2P_{\perp} + P'_{\perp})^2 \sinh^2(\gamma - \gamma') - (P_{\parallel} - P'_{\parallel})^2 \cosh^2(\gamma - \gamma')}}}, \tag{103}$$

$$(3P_{\perp} + P_{\parallel})(3P'_{\perp} + P'_{\parallel}) \cosh(2\gamma - 2\gamma') = P_{\perp}(P'_{\parallel} + 4P_{\perp}) + P'_{\perp}(2P'_{\parallel} + P_{\perp}) + 4P'^2_{\perp} + P_{\parallel}(P'_{\parallel} + 2P_{\perp} + P'_{\perp}), \tag{100}$$

Similarly to the example from relativistic hydrodynamics, consider the case when the normal vector is directed along

the Ox -axis $N^\mu = (0, 1, 0, 0)$, then from the Eqs. (91–92) we find expressions for the velocities u_x, u'_x :

$$\sinh \gamma = u_x = \sqrt{\frac{(P_\perp - P'_\perp)(P'_\parallel + P_\perp + 2P'_\perp)}{(2P_\perp - P_\parallel - 2P'_\perp + P'_\parallel)(P'_\parallel + 2P_\perp + P'_\perp)}}, \quad (104)$$

$$\sinh \gamma' = u'_x = \sqrt{\frac{(P_\perp - P'_\perp)(P'_\parallel + 2P_\perp + P'_\perp)}{(2P_\perp - P_\parallel - 2P'_\perp + P'_\parallel)(P'_\parallel + P_\perp + 2P'_\perp)}}, \quad (105)$$

References

1. F. Gelis, Some aspects of the theory of heavy ion collisions (2021). [arXiv:2102.07604](https://arxiv.org/abs/2102.07604) [hep-ph]
2. T. Lappi, L. McLerran, Some features of the glasma. *Nucl. Phys. A* **772**, 200–212 (2006). <https://doi.org/10.1016/j.nuclphysa.2006.04.001> [arXiv:hep-ph/0602189](https://arxiv.org/abs/hep-ph/0602189)
3. R. Baier, P. Romatschke, U.A. Wiedemann, Dissipative hydrodynamics and heavy ion collisions. *Phys. Rev. C* **73**, 064903 (2006). <https://doi.org/10.1103/PhysRevC.73.064903> [arXiv:hep-ph/0602249](https://arxiv.org/abs/hep-ph/0602249)
4. P. Romatschke, New Developments in Relativistic Viscous Hydrodynamics. *Int. J. Mod. Phys. E* **19**, 1–53 (2010). <https://doi.org/10.1142/S0218301310014613> [arXiv:0902.3663](https://arxiv.org/abs/0902.3663) [hep-ph]
5. S. Jeon, U. Heinz, Introduction to Hydrodynamics. In: *Quark-Gluon Plasma 5*, ed. by Xin-Nian Wang, pp. 131–187 (2016). https://doi.org/10.1142/9789814663717_0003
6. M. Martinez, M. Strickland, Dissipative dynamics of highly anisotropic systems. *Nucl. Phys. A* **848**, 183–197 (2010). <https://doi.org/10.1016/j.nuclphysa.2010.08.011>
7. W. Florkowski, R. Ryblewski, Highly anisotropic and strongly dissipative hydrodynamics with transverse expansion. *Eur. Phys. J. C* **71**(11), 1761 (2011). <https://doi.org/10.1140/epjc/s10052-011-1761-8>
8. W. Florkowski, R. Ryblewski, A. Hydrodynamics, Three Lectures. *Acta Phys. Polon. Ser. B* **45**(12), 2355–2394 (2011). <https://doi.org/10.5506/APhysPolB.45.2355>
9. M. Alqahtani, M. Nopoush, M. Strickland, Relativistic anisotropic hydrodynamics. *Prog. Part. Nucl. Phys.* **101**, 204–248 (2018). <https://doi.org/10.1016/j.pnpnp.2018.05.004> [arXiv:1712.03282](https://arxiv.org/abs/1712.03282) [nucl-th]
10. M. Alqahtani et al., Anisotropic hydrodynamic modeling of heavy-ion collisions at LHC and RHIC. *Nucl. Phys. A* **982**, 423–426 (2019). <https://doi.org/10.1016/j.nuclphysa.2018.10.066> [arXiv:1807.05508](https://arxiv.org/abs/1807.05508) [hep-ph]
11. A.V. Leonidov, On nonadditive anisotropic relativistic hydrodynamics. *JETP Lett.* **113**(9), 599–601 (2021). <https://doi.org/10.1134/S0021364021090010> [arXiv:2102.10819](https://arxiv.org/abs/2102.10819) [nucl-th]
12. M. Kirakosyan, A. Kovalenko, A. Leonidov, Sound propagation and Mach cone in anisotropic hydrodynamics. *Eur. Phys. J. C* **79**(5), 434 (2019). <https://doi.org/10.1140/epjc/s10052-019-6919-9> [arXiv:1810.06122](https://arxiv.org/abs/1810.06122) [hep-ph]
13. L.D. Landau, E. MikhailovichLifshitz, *Course of theoretical physics. Hydrodynamics* (Elsevier, Amsterdam, 2013)
14. W. Israel, Relativistic theory of shock waves. *Proc. R. Soc. Lond. A* **259**(1296), 129–143 (1960)
15. T.P. Mitchell, D.L. Pope, Shock waves in an ultra-relativistic fluid. *Proc. R. Soc. Lond. A* **277**(1368), 24–31 (1964)
16. A. Majorana, S. Motta, Shock structure in relativistic fluid-dynamics. *J. Non-Equilib. Thermodyn.* **10**(1), 29–36 (1985). <https://doi.org/10.1515/jnet.1985.10.1.29>
17. T.S. Olson, W.A. Hiscock, Plane steady shock waves in Isreal-Stewart fluids. *Ann. Phys.* **204**(2), 331–350 (1990). [https://doi.org/10.1016/0003-4916\(90\)9039](https://doi.org/10.1016/0003-4916(90)9039)
18. W. Scheid, H. Muller, W. Greiner, Nuclear shock waves in heavy-ion collisions. *Phys. Rev. Lett.* **32**, 741–745 (1974). <https://doi.org/10.1103/PhysRevLett.32.741>
19. A.M. Gleeson, S. Raha, Shock waves in relativistic nuclear matter I. *Phys. Rev. C* **21**, 1065–1077 (1980). <https://doi.org/10.1103/PhysRevC.21.1065>
20. A.M. Gleeson, S. Raha, Shock waves in relativistic nuclear matter 2 angular anisotropy in multiparticle spectra. *Phys. Rev. C* **26**, 1521 (1982). <https://doi.org/10.1103/PhysRevC.26.1521>
21. M. Gyulassy, D.H. Rischke, B. Zhang, Transverse shocks in the turbulent gluon plasma produced in ultrarelativistic A+A. In: *International Conference on Nuclear 19 Physics at the Turn of Millennium: Structure of Vacuum and Elementary Matter*. Mar. 1996, pp. 427–434. [arXiv:nucl-th/9606045](https://arxiv.org/abs/nucl-th/9606045)
22. M. Gyulassy, D. Rischke, B. Zhang, Hot spots and turbulent initial conditions of quark - gluon plasmas in nuclear collisions. *Nucl. Phys. A* **613**, 397–434 (1997). [https://doi.org/10.1016/S0375-9474\(96\)00416-2](https://doi.org/10.1016/S0375-9474(96)00416-2) [arXiv:nucl-th/9609030](https://arxiv.org/abs/nucl-th/9609030)
23. P. Romatschke, M. Strickland, Collective modes of an anisotropic quark-gluon plasma. *Phys. Rev. D.* **68**, 036004 (2003). <https://doi.org/10.1103/PhysRevD.68.036004>
24. P. Romatschke, M. Strickland, Collective modes of an anisotropic quark-gluon plasma II. *Phys. Rev. D.* **70**, 116006 (2004). <https://doi.org/10.1103/PhysRevD.70.116006>